



Cite this: *Soft Matter*, 2016,  
12, 5438

Received 10th May 2016,  
Accepted 23rd May 2016

DOI: 10.1039/c6sm01098a

[www.rsc.org/softmatter](http://www.rsc.org/softmatter)

## Nematic ordering of semiflexible polymers confined on a toroidal surface

Shiwei Ye,<sup>a</sup> Pingwen Zhang<sup>\*a</sup> and Jeff Z. Y. Chen<sup>\*b</sup>

We study the isotropic-like and nematic states of wormlike liquid-crystal polymers embedded on the surface of a torus. The role played by surface curvature, which couples to the molecular rigidity, is reported as the main reason that causes the weak nematic ordering in an otherwise ordinary isotropic phase. The same coupling has a profound effect on the nematic states as well, which are stabilized by the Onsager excluded-volume interaction; the latter has been frequently used to study lyotropic liquid crystal polymers and is used here as an example of the physical mechanisms that drive the system to make orientational ordering. We identify important parameters in the system which are used as axes of the four-dimensional phase diagram. The numerical study demonstrates a strong correlation between the liquid-crystal defect-free and defect structures and the geometry of the liquid-crystal embedded surface.

### 1 Introduction

The structure of surface-confined liquid crystals has drawn significant theoretical and experimental attentions in recent years. Depending on the geometry of the confining surface, the system may display both density and orientational field defects, which can be detected experimentally.<sup>1–7</sup> The nature of an ordered state depends on the geometric parameters as well as how far the system is away from the isotropic-nematic transition. One frequently used example in theories and computer simulations is the nematic defect structure formed by a two-dimensional fluid containing liquid-crystal molecules confined on a spherical surface.<sup>1,8–17</sup>

A distinctive feature of a toroidal surface is that it is not a geometrical shape that frustrates the nematic-director field. Mathematically, its Euler characteristic of the manifold is zero, hence any embedded director field has either no defect or a defect pattern that must have all winding numbers summed up to zero.<sup>18</sup> However, the toroidal surface provides an interesting playground for the interplay between the local surface curvature and the distorted nematic surface. Unlike the uniform curvature on a spherical surface, on a toroidal surface the curvature depends on the location of the considered point and the tangent direction at which a molecular segment points.

A number of theoretical and computer-simulation approaches have been taken to study nematic structures in confinement. The Frank elastic and Landau-de Gennes free-energy models are often

used and contain phenomenological parameters.<sup>1,8–10,13,19–21</sup> The molecular-level based models, either the simpler Onsager and Maier-Saupe theories, or the more complicated density-functional theories, contain system parameters that can be traced back to the physical origins.<sup>14,15,17,22–27</sup>

Previous studies of liquid crystals confined on a toroidal surface are mostly based on simplified versions of the Frank-energy model. Studying the Frank energy in a covariant form, Evans reported that structural defects can be stabilized in a system containing molecules displaying *p*-atic orderings on a toroidal membrane surface.<sup>28</sup> Bowick *et al.* investigated the liquid-crystal patterns generated by hexatic ordering on a toroidal surface, developing a general comparison between the defect-substrate interaction with the electrostatic interaction.<sup>29</sup> Selinger *et al.* treated the variation of the directional ordering in a Frank energy by a full three-dimensional derivative on a toroidal surface, which can be directly transformed into a surface XY-spin model in addition to an energy penalty.<sup>30</sup> Using the same Frank energy on a toroidal surface, Li *et al.* examined the structure of the defect-free nematic states and revealed that multiple nematic states can exist in this system; a simulated annealing Monte Carlo method was used to obtain the free energy minima in this work.<sup>21</sup> Segatti *et al.* investigated the stable states that can be obtained from the Frank-energy model and also discovered different defect-free nematic states;<sup>31</sup> their analysis combined methods from differential geometry, topology, functional analysis, and numerical solutions. Jesenek *et al.* calculated the liquid-crystal defect patterns using a two-dimensional Landau-de Gennes free-energy expansion on the order-parameter tensor, with and without the consideration of the surface-curvature effects.<sup>32</sup> In all these studies except for the last one, it is

<sup>a</sup> LMAM and School of Mathematical Sciences, Peking University, Beijing, 100871, People's Republic of China. E-mail: pzhang@pku.edu.cn

<sup>b</sup> Department of Physics and Astronomy, University of Waterloo, Waterloo, Ontario, N2L 3G1, Canada. E-mail: jeffchen@uwaterloo.ca

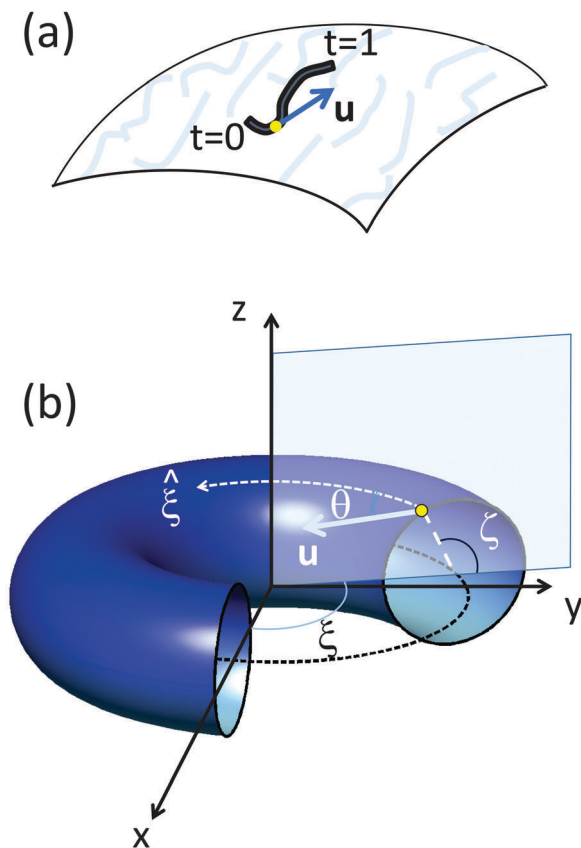


**Fig. 1** (a) Illustration of liquid-crystal polymers on a curved surface and (b) coordinate system used for a toroidal surface of axial radius  $R$  and revolving-ring radius  $r$ . A point on the two-dimensional toroidal surface is specified by two angular variables,  $\xi$  and  $\zeta$ . In the current work, the direction of a polymer segment is specified by a unit vector  $\mathbf{u}$ , which makes an angle  $\theta$  with respect to the normal of a constant  $\xi$  plane.

assumed that the system can be described by a single Frank constant  $K$ . The importance of a curvature related bending-energy term for studying liquid crystals on a curved surface was first emphasized by Selinger *et al.* with  $K$  as the coefficient.<sup>30,33,34</sup>

One of the main contributions of the current work is to identify the molecular origin of such a bending-energy term (see Section 2.3). We study a system composed of  $n$  semi-flexible polymer chains. Following a series of work on liquid-crystal polymers in spatially homogeneous and inhomogeneous systems,<sup>35–42</sup> here the same self-consistent field theory (SCFT) is used to treat wormlike polymer chains, now confined on a toroidal surface. The theory takes the Onsager excluded volume into account and yields the rigid-rod and flexible-chain limits by adjusting the polymer-length to persistence-length ratio.<sup>43</sup> The formalism is briefly reviewed in Section 2.1. Using the coordinate system in Fig. 1, in Section 2.2 we produce the necessary mathematical structure, for wormlike liquid crystal chains confined on a toroidal surface, in particular. Rather than the phenomenological parameters (e.g., the Frank constants), four system-parameters are identified in the current model, each having physical

significance at the molecular level. This is summarized in Section 3.1.

The origin of the curvature related bending-energy term from this derivation is physically transparent – it is directly equal to the bending-energy cost of confining semiflexible molecules on a toroidal surface. In comparison, the bending energy term yielded from the Frank-energy model is related to bending a surface element. This simple difference has a fundamental consequence: the bending-energy term derived here is related to square normal curvature of a line element along a direction, whereas the bending-energy term in ref. 21, 30–32 is related to the surface curvature tensor. Details are discussed in Section 2.3.

Another main contribution of the current work is to show that a pure isotropic state does not exist anymore, even below the traditional isotropic-nematic transition. Most previous studies treated the nematic states by making the assumption that a liquid-crystal ordering already exists, with no attention paid to the isotropic state.<sup>21,28–32</sup> As it turns out, an isotropic-like state of this system possesses a weak nematic orientational ordering. The physical mechanism that drives this weak nematic ordering is quite different from a typical nematic state – the directional ordering is directly caused by the local curvature coupling. This is addressed in Section 3.3, where two isotropic-like states are identified.

As the molecular density increases, the system undergoes a traditional isotropic-like-to-nematic phase transition, due to the preferred molecule–molecule interaction represented here by the Onsager interaction. This is in concert with the phase transition seen in a bulk problem. On toroidal surface, however, the interplay between geometric effects, molecular density, and molecular semi-flexibility yields three low-free-energy nematic states; each has its own orientational characteristics, as explained in Section 3.4. The analysis verifies the existence of multiple nematic states recently identified in ref. 21, 31 and 32. In Section 3.5 we describe the four-dimensional phase diagram which divides the phase space into regions where these states are stable.

The analysis carried out here is based on a free-energy model that contains a density distribution as a function of both spatial position and molecular orientation. Such a formalism is capable of producing real defects in both orientational and density fields, where a defect is related to a singularity in the density distribution function. This can be contrasted to the tool used in a Frank-energy model where a unit-vector field (the nematic-director field) is the main focus. Because of the unit-vector nature, a defect point cannot be described by a continuous variation of the field, rather, often represented by a disclination of the vector field. In Section 3.6 we describe the various defect structures found in this work, verifying previous findings.<sup>21,30,32</sup> Because the defect energy can be clearly estimated in our model, in the same section we discuss the metastability of these defect states.

The theoretical formalism and a discussion on the surface curvature effects are contained in Section 2. Readers who are not interested in the theoretical and mathematical details can directly skip to Section 3.

## 2 Free energy of wormlike liquid crystal polymers on curved surface

### 2.1 General formalism

The basic liquid-crystal model in this study is made of  $n$  wormlike polymer chains which are confined on a closed surface of a total area  $A$ . The reduced surface chain density is then

$$\sigma \equiv nL^2/A, \quad (1)$$

where  $L$  is the total contour length of a polymer. In this section we describe the free energy yielded from a self-consistent field theory, taking the Onsager excluded-volume interaction into account.

The configuration of a polymer chain is described by the coordinate vector  $\mathbf{r}(t)$  where  $t$  is an arc-variable that continuously varies from  $t = 0$  at one end to  $t = 1$  at another end. The tangent direction of a chain segment at  $t$  is specified by  $\mathbf{u}(t) \equiv L^{-1}d\mathbf{r}/dt$  [see Fig. 1]. The statistical weight for the chain configuration is assumed to be<sup>44</sup>

$$P[\mathbf{r}(t)] = \exp \left\{ -\frac{\lambda}{2L} \int_0^1 dt \left| \frac{d\mathbf{u}(t)}{dt} \right|^2 - \int_0^1 dt W[\mathbf{r}(t), \mathbf{u}(t)] \right\}, \quad (2)$$

where  $\lambda$  is the bare persistence length, defined through the orientation–orientation correlation function of a free wormlike polymer in three-dimensional space. At this stage,  $W$  is the mean potential field acting on the chain under consideration from the neighboring polymer chains.

Let  $\phi(\mathbf{r}, \mathbf{u})$  be the dimensionless probability function to find any polymer segment, which has a tangent vector pointing at the direction of the unit vector  $\mathbf{u}$ , at a location specified by the vector  $\mathbf{r}$ . The function is normalized according to

$$\frac{1}{A} \int d\mathbf{r} d\mathbf{u} \phi(\mathbf{r}, \mathbf{u}) = 1. \quad (3)$$

Within SCFT, the reduced free energy per polymer chain can be written as

$$\begin{aligned} \tilde{F} &= \frac{1}{nk_B T} F[\phi(\mathbf{r}, \mathbf{u}), W(\mathbf{r}, \mathbf{u})] = \ln \left( \frac{\sigma A}{Q} \right) \\ &+ \frac{1}{A} \int d\mathbf{r} d\mathbf{u} [-W(\mathbf{r}, \mathbf{u}) \phi(\mathbf{r}, \mathbf{u})] \\ &+ \frac{\sigma}{2} \int d\mathbf{u}' \phi(\mathbf{r}, \mathbf{u}) |\mathbf{u} \times \mathbf{u}'| \phi(\mathbf{r}, \mathbf{u}'), \end{aligned} \quad (4)$$

where  $W(\mathbf{r}, \mathbf{u})$  is a mean field introduced to represent the average effects of polymers on a representative chain. Here,  $k_B$  is the Boltzmann constant and  $T$  temperature. The free energy expression in (4) is a functional of two yet-to-be determined functions,  $\phi(\mathbf{r}, \mathbf{u})$  and  $W(\mathbf{r}, \mathbf{u})$ . The last term is the result of generalizing the Onsager interaction for rodlike molecules to a wormlike liquid-crystal system.<sup>43,45,46</sup> Taking rodlike particles confined on a surface as an example, we can show that the excluded-volume between two rods is proportional to  $L^2$  and the rod width (assumed much smaller than  $L$ ) does not enter into the excluded-area expression.<sup>43</sup> In any case,  $\sigma$  represents the

magnitude of the directionally-dependent molecule–molecule interaction.

The single-chain partition function  $Q$  in the above expression can be calculated from the propagator  $q(\mathbf{r}, \mathbf{u}; t)$ ,

$$Q = \int d\mathbf{r} d\mathbf{u} q(\mathbf{r}, \mathbf{u}; 1). \quad (5)$$

The propagator itself is a reduced Green's function that represents the probability of finding the terminal point of polymer segment of length  $t$  to appear at a spatial position located at  $\mathbf{r}$  and to point at a direction specified by  $\mathbf{u}$ . One can show, based on the configurational probability assumed in (2), that the propagator satisfies a differential equation<sup>47,48</sup>

$$\frac{\partial}{\partial t} q(\mathbf{r}, \mathbf{u}, t) = \left[ -W(\mathbf{r}, \mathbf{u}) - \frac{L\lambda}{2} \kappa^2(\mathbf{r}, \mathbf{u}) - L\mathbf{u} \cdot \nabla_{\mathbf{r}} \Big|_{\mathbf{u}} + \frac{L}{2\lambda} \nabla_{\mathbf{u}}^2 \right] q(\mathbf{r}, \mathbf{u}, t), \quad (6)$$

with an initial condition  $q(\mathbf{r}, \mathbf{u}, 0) = 1$ . All derivatives are taken in a covariant form on the surface of consideration. In particular,  $\nabla_{\mathbf{r}}$  is treated with the  $\mathbf{u}$  vector fixed in space.

The rigorous derivation of eqn (6) based on (2) can be found in ref. 43 and 48. Here we note that  $\kappa^2(\mathbf{r}, \mathbf{u})$  is the square normal curvature along direction  $\mathbf{u}$  on a surface of arbitrary shape. The term  $L\lambda\kappa^2(\mathbf{r}, \mathbf{u})/2$  comes from the energy penalty to bend a polymer segment on the surface along direction  $\mathbf{u}$ ; for a given geometry it has a specific form. Using vector analysis, we have

$$\kappa^2 = |[(\mathbf{u} \cdot \nabla_{\mathbf{r}}) \mathbf{N}(\mathbf{r})] \times (\mathbf{u} \times \mathbf{N})|^2, \quad (7)$$

where  $\mathbf{N}(\mathbf{r})$  is the normal vector of a surface element located at position vector  $\mathbf{r}$ . A simpler version of  $\kappa^2$  is given in Section 2.3.

Minimization of the free energy with respect to  $\phi(\mathbf{r}, \mathbf{u})$  yields

$$W(\mathbf{r}, \mathbf{u}) = \sigma \int d\mathbf{u}' |\mathbf{u} \times \mathbf{u}'| \phi(\mathbf{r}, \mathbf{u}'), \quad (8)$$

and minimization of the free energy with respect to  $W(\mathbf{r}, \mathbf{u})$  yields

$$\phi(\mathbf{r}, \mathbf{u}) = \frac{A}{Q} \int_0^1 dt q(\mathbf{r}, \mathbf{u}, t) q(\mathbf{r}, -\mathbf{u}, 1-t). \quad (9)$$

The equation set, from (5) to (9), forms complete self-consistent equations that need to be solved.

### 2.2 Wormlike liquid crystals confined on a toroidal surface

In this subsection we set up a covariant coordinate system on a toroidal surface that is described by two radii: the toroidal circular-axis-to-center radius  $R$  and the torus cross-section radius  $r$ . A point on the toroidal surface can be described by two angular parameters  $\xi$  and  $\zeta$  as shown in Fig. 1(b). The unit vector  $\mathbf{u}$  is specified by the angle  $\theta$  shown in the figure. In the rest of this paper, we reduce all length variables and parameters by  $r$ . For example, the radius  $R$ , is now specified through

$$k^{-1} \equiv R/r, \quad (10)$$

and the total surface area is  $A = r^2 \int_0^{2\pi} d\xi \int_0^{2\pi} (k^{-1} + \cos \zeta) d\zeta = 4\pi^2 r^2 k^{-1}$ .

Within this coordinate system, a point on the torus surface is written in Cartesian coordinates,

$$\mathbf{r}/r = (k^{-1} + \cos \zeta) \cos \xi \hat{x} + (k^{-1} + \cos \zeta) \sin \xi \hat{y} + \sin \zeta \hat{z}. \quad (11)$$

The directional unit vector is written

$$\mathbf{u} = \hat{\xi} \cos \theta + \hat{\zeta} \sin \theta, \quad (12)$$

where the axis unit vectors are

$$\hat{\xi} = -\sin \xi \hat{x} + \cos \xi \hat{y}, \quad (13)$$

and

$$\hat{\zeta} = -\cos \xi \sin \zeta \hat{x} - \sin \xi \sin \zeta \hat{y} + \cos \zeta \hat{z}. \quad (14)$$

The operators in (6) can then be expressed by

$$\nabla_{\mathbf{u}}^2 = \frac{\partial^2}{\partial \theta^2}. \quad (15)$$

The operate  $\mathbf{u} \cdot \nabla_{\mathbf{r}}|_{\mathbf{u}}$  needs to be performed with care, as fixing the direction vector  $\mathbf{u}$  in a curvilinear coordinate system is not the same as fixing the direction variable such as  $\theta$ . One can write  $\mathbf{u} \cdot \nabla_{\mathbf{r}}|_{\mathbf{u}} = \mathbf{u} \cdot \nabla_{\mathbf{r}} - [(\mathbf{u} \cdot \nabla_{\mathbf{r}} \mathbf{u}) \cdot \nabla_{\mathbf{u}}]$  where the derivatives of all terms on the right-hand side are taken with respect to the variables and  $\nabla_{\mathbf{r}} \mathbf{u}$  is taken on the rotating unit axis-vectors of  $\mathbf{u}$ .<sup>43,48</sup> We then have

$$\mathbf{u} \cdot \nabla_{\mathbf{r}}|_{\mathbf{u}} = \frac{1}{r} \left[ \frac{\cos \theta}{(k^{-1} + \cos \theta)} \frac{\partial}{\partial \xi} + \sin \theta \frac{\partial}{\partial \zeta} - \frac{\cos \theta \sin \zeta}{\cos \zeta + k^{-1} \partial \theta} \frac{\partial}{\partial \theta} \right]. \quad (16)$$

According to eqn (7) the square curvature is expressed by

$$\kappa^2 = \frac{1}{r^2} \left[ \frac{\sin^2 \theta + k \cos \zeta}{k \cos \zeta + 1} \right]^2. \quad (17)$$

Once the propagator is solved, the single chain partition function is found from

$$Q = r^2 \int d\xi d\zeta d\theta q(\xi, \zeta, \theta, 1)(k^{-1} + \cos \zeta). \quad (18)$$

### 2.3 Curvature energy penalty and covariant form

The theoretical formalism in this work is written by using  $W$  as a mean field. We can rewrite the equation in another representation that makes the curvature energy penalty in a more identifiable form.

The starting point is to define a new field,

$$W'(\mathbf{r}, \mathbf{u}) = W(\mathbf{r}, \mathbf{u}) + \frac{L\lambda}{2} \kappa^2(\mathbf{r}, \mathbf{u}). \quad (19)$$

Using it in the free-energy-per-chain expression before minimization, (4), we obtain

$$\begin{aligned} \tilde{F}[\phi(\mathbf{r}, \mathbf{u}), W(\mathbf{r}, \mathbf{u})] &= \tilde{F}[\phi(\mathbf{r}, \mathbf{u}), W'(\mathbf{r}, \mathbf{u})] \\ &+ \frac{L\lambda}{2A} \int d\mathbf{r} d\mathbf{u} \kappa^2(\mathbf{r}, \mathbf{u}) \phi(\mathbf{r}, \mathbf{u}). \end{aligned} \quad (20)$$

The propagator equation becomes

$$\frac{\partial}{\partial t} q(\mathbf{r}, \mathbf{u}, t) = \left[ -W'(\mathbf{r}, \mathbf{u}) - L\mathbf{u} \cdot \nabla_{\mathbf{r}}|_{\mathbf{u}} + \frac{L}{2\lambda} \nabla_{\mathbf{u}}^2 \right] q(\mathbf{r}, \mathbf{u}, t). \quad (21)$$

The mathematical structure of these two expressions is such that a bending penalty term is added to the otherwise covariant theory formed by (21) and the first term in (20).

Using the Frank-energy model for liquid crystals that contains the covariant-derivatives only,<sup>49,50</sup> Evans studied the structure of possible structural defects of surface-embedded liquid-crystals on a toroidal membrane surface.<sup>28</sup> On the other hand, Selinger, Konya, Travesset and Selinger (SKTS) treated the variation of the directional ordering by a full three-dimensional derivative on the toroidal surface.<sup>30</sup> Within the assumption of one Frank elastic constant, the difference between the two models can be viewed from

$$F_{\text{SKTS}} = F_{\text{Evans}} + K \int (\mathbf{n} \cdot \mathbf{K} \cdot \mathbf{K} \cdot \mathbf{n}) d\mathbf{r} \quad (22)$$

where  $K$  is the Frank elastic constant,  $\mathbf{n}(\mathbf{r})$  is the nematic director field assumed in the Frank-energy theory, and  $\mathbf{K}$  is the surface curvature tensor.<sup>30</sup> Eqn (22) can be directly compared with (20). The similarity is that both contain the curvature effects as an addition to a covariant model.

However there are some major differences between (20) and (22). First, we note that the bare persistence length  $\lambda$  is directly proportional to the bending energy of a wormlike chain.<sup>43,44</sup> The origin of the last term in (20) stems from the bending energy of placing a typical polymer on the curved surface. In the more flexible case where  $\lambda \ll L$ , the coefficient  $L\lambda$  is proportional to the mean square radius of gyration of a polymer in a free space. This term then becomes the energy needed to bend and shape an originally free polymer to fit to the local curvature of the embedding surface. In the rigid limit where  $\lambda \ll L$ , this term reflects the reality that it is hard to bend a rigid molecule to suit a large local surface curvature; as a result, molecules prefer to align themselves along the direction of a lower curvature. Within the Frank energy,  $K$  is a phenomenological parameter that deals with the bending of the nematic texture, represented by the director field, on a curved surface.

Second,  $\kappa$  in eqn (7) is the normal curvature at a surface point where a surface-embedded curve passes with a tangent direction  $\mathbf{u}$ . This is the direct consequence of bending a polymer (a curve) on a surface. In differential geometry, it is defined by the first and second fundamental forms of surface differentials. According to the Euler curvature formula,

$$\kappa^2 = (\kappa_1 \cos^2 \theta + \kappa_2 \sin^2 \theta)^2 \quad (23)$$

where  $\kappa_1$  and  $\kappa_2$  are the two principal curvatures, in our case along  $\hat{\xi}$  and  $\hat{\zeta}$ ,

$$\kappa_1 = \frac{\cos \zeta}{R + r \cos \zeta} \text{ and } \kappa_2 = \frac{1}{r}. \quad (24)$$

The angle  $\theta$  is defined in (12). One can directly verify the expression in eqn (17), which is obtained from the more

involved expression in eqn (7), by substituting these principal curvatures into eqn (23).

In contrast,  $\mathbf{K}$  appearing in (22) is the surface curvature tensor, the tensor form of the so-called shape operator. As a surface property, it is defined through the third fundamental form and is independent of  $\mathbf{u}$ . This is a natural form appearing in the Frank-energy model, as it deals with a bending surface element. The projection to  $\mathbf{u}$  takes place when the last term is considered in (22). In a diagonalized  $\mathbf{K}$ , the diagonal elements are  $\kappa_1$  and  $\kappa_2$ , respectively. Hence

$$\mathbf{n} \cdot \mathbf{K} \cdot \mathbf{n} = \kappa_1^2 \cos^2 \theta + \kappa_2^2 \sin^2 \theta = \kappa_1^2 + (\kappa_2^2 - \kappa_1^2) \sin^2 \theta \quad (25)$$

with the assumption that the vector  $\mathbf{n}$  makes an angle  $\theta$  with  $\hat{\zeta}$ , locally. Apart from the unimportant constant  $\int \kappa_1^2 d\mathbf{r}$ , the last term above is exactly the expression used in eqn (9) of ref. 21 and yet apart from another constant, eqn (8) of ref. 31. Hence, originated from the different starting points, bending a curve and bending a surface element, the energy penalty term appearing in the current work is different from the energy penalty used in ref. 21, 30 and 31. Qualitatively, results on the nematic structures yielded from the two approaches are similar, as described below.

Third, as we show below, instead of the completely isotropic state, there exists isotropic-like states. While the last term in (20) contains the consideration of a distribution of molecular segments along all directions, the last term in (22) is written for the nematic direction only. This is a particularly interesting point here, as we see below, (22) lacks a mechanism to describe the weak orientational distribution of an isotropic-like state. As we describe the nematic defect patterns in a later section, (20) can be used for calculating the defect energy, whereas (22) can not be used for calculating the disclination of the nematic field at the singularity.

Finally we remark that the last term in (20) is independent of the orientationally dependent interactions between polymer segments. To showcase the usefulness of the model, we adopt the Onsager interaction, the last term in (4), following the tradition of a series of studies on the subject of liquid-crystal polymers.<sup>45,46,51</sup> One could study wormlike polymer liquid crystals, replacing the Onsager interaction by, for example, the Maier-Saupe free energy<sup>50,52-54</sup> or replacing the Onsager interaction by a more complicated density-functional theory.<sup>22-25</sup>

### 3 Orientational ordering on a toroidal surface

#### 3.1 System parameters

Here we identify the essential parameters that appear in the model described in the last section. Within the theory the orientational structure of the wormlike polymer fluid on the toroidal surface depends on four parameters:

(a) Bending-energy coefficient

$$\gamma = L\lambda/2r^2 \quad (26)$$

from the coefficient of a reduced  $\kappa^2$  in (6). It is a system parameter that competes with, for example, the entropy coefficient  $L/2\lambda$  and the coefficient of the Onsager interaction  $\sigma$ .

(b) The reduced polymer density  $\sigma$  defined in (1), which appears as the coefficient of the Onsager interaction term in (4). In a typical lyotropic system,<sup>55</sup> a low- $\sigma$  system is in an isotropic state and a high- $\sigma$  system is in a nematic state. Within the same theoretical foundation, one can determine the critical surface density of an isotropic-nematic transition on a two-dimensional flat surface, by removing the  $\nabla_{\mathbf{r}}$  and  $\kappa^2$  terms in eqn (6). As a function of  $L/\lambda$ , the transition density is  $\sigma^* = 3\pi/4A_1(L/\lambda)$  where  $A_1(L/\lambda) = (\lambda/2L)[1 + (\lambda/2L)(e^{-2L/\lambda} - 1)]$ . This was determined in terms of an effective two-dimensional Kuhn length in ref. 51 and reviewed in terms of the persistence length in ref. 43.

(c) The geometric ratio  $k$  defined in (10), which appears in (6). The same parameter was used in the Frank-energy models<sup>21,30,31</sup> and in the Landau-de Gennes model.<sup>32</sup> It has the characteristic parameter for a torus and has the parameter range [0,1]. That different defect-free nematic states can be obtained from varying  $k$  was shown previously.<sup>21,31,32</sup>

(d) The flexibility of the polymers in the system,

$$\alpha = L/2\lambda, \quad (27)$$

which appears as a coefficient of the last term on the right-hand side in (6). It is a characteristic measure of a free polymer. The  $L/\lambda \ll 1$  limit corresponds to rodlike molecules and  $L/\lambda \gg 1$  flexible molecules. In three dimensions,  $2\lambda$  can be identified with the effective Kuhn length. The parameter defined above is consistent with the definition of the degree of polymerization (ratio between the total length and Kuhn length) in three dimensions. Note that the coefficient of the coupling term,  $L/r$  in (6) is not an independent system parameter. It is related to other parameters by  $L/r = \sqrt{2\gamma L/\lambda}$ .

All these four system parameters can be traced back to the physics at a molecular level.

#### 3.2 Order parameter and nematic director

Within the current coordinate set up, the density distribution function  $\phi(\mathbf{r}; \mathbf{u})$  is expressed by  $\phi(\xi, \zeta; \theta)$ . We can then examine two characteristic quantities of orientational ordering as functions of the location: the main order parameter  $S(\xi, \zeta)$  and the direction of the nematic director  $\theta_m(\xi, \zeta)$ , at which the distribution function  $\phi(\xi, \zeta; \theta)$  has a maximum in  $\theta$ .

To calculate these quantities, on a two-dimensional surface, we define the orientational order parameter tensor

$$Q(\xi, \zeta) = \begin{bmatrix} Q_1(\xi, \zeta) & Q_3(\xi, \zeta) \\ Q_3(\xi, \zeta) & Q_2(\xi, \zeta) \end{bmatrix}, \quad (28)$$

which should not be confused with the notation  $Q$  used for the partition function. The elements in the matrix are defined by

$$Q_1(\xi, \zeta) = \int_0^{2\pi} \left( \cos^2 \theta - \frac{1}{2} \right) \phi(\xi, \zeta, \theta) d\theta / \phi(\xi, \zeta), \quad (29)$$

$$Q_2(\xi, \zeta) = \int_0^{2\pi} \left( \sin^2 \theta - \frac{1}{2} \right) \phi(\xi, \zeta, \theta) d\theta / \phi(\xi, \zeta),$$

and

$$Q_3(\xi, \zeta) = \int_0^{2\pi} \cos \theta \sin \theta \phi(\xi, \zeta, \theta) d\theta / \phi(\xi, \zeta), \quad (30)$$

where

$$\phi(\xi, \zeta) = \int_0^{2\pi} \phi(\xi, \zeta, \theta) d\theta \quad (31)$$

is the overall molecular fraction at a specific location.

Based on this definition, the main order parameter measured from a local nematic director  $\mathbf{n}(\xi, \zeta)$  is found from diagonalizing the  $Q$  tensor,

$$S(\xi, \zeta) = 2\sqrt{Q_1^2(\xi, \zeta) + Q_3^2(\xi, \zeta)}. \quad (32)$$

The director field itself is specified from

$$\mathbf{n}(\xi, \zeta) = \hat{\xi} \cos \theta_m(\xi, \zeta) + \hat{\zeta} \sin \theta_m(\xi, \zeta) \quad (33)$$

where  $\theta_m$  is calculated by

$$\cos \theta_m(\xi, \zeta) = \frac{1}{2} + \frac{Q_1(\xi, \zeta)}{S(\xi, \zeta)}. \quad (34)$$

When the distribution function has a strong peak along the direction  $\mathbf{n}$ ,  $S \sim 1$ . When the distribution function is isotropic,  $S = 0$ . However, we remark that on a curved surface, there is no ideal isotropic state.

### 3.3 Isotropic-like states

On a flat two-dimensional space,  $\kappa = 0$ , the low- $\sigma$  state is an isotropic state with no orientational ordering. The system makes a continuous phase transition to a nematic state at a critical  $\sigma$ ; this has been well documented previously.<sup>51</sup> Here, however, due to the curvature effects, there is no pure isotropic state. As it turns out, depending on the geometric ratio  $k$ , there are two low- $\sigma$  states that have a weak, regional nematic ordering. These states can be traced back to the isotropic state as we take  $\kappa \rightarrow 0$  asymptotically. Strictly speaking, these isotropic-like states are (weak) nematic states.

As our first example, we consider the case of  $\sigma = 0$ ,  $\alpha = L/2\lambda \ll 1$ , with a fixed, moderate  $\gamma$ . Note in this case  $L/r \ll 1$ . Basically, we have a dilute rodlike system containing almost rigid molecules which are confined on a toroidal surface with a small rod-length to  $r$ -radius ratio. Dropping the first, third, and fourth terms on the right-hand side of (6), we obtain an analytic solution for  $q$ . Carrying out all necessary integrations, we finally obtain the distribution function

$$\phi(\xi, \zeta; \theta) = \frac{\exp(-\gamma \bar{\kappa}^2)}{Q} \quad (35)$$

where  $\bar{\kappa}^2 \equiv r^2 \kappa^2$  is a dimensionless version of (17), which depends on  $\zeta$  and  $\theta$  only. Hence we see that the distribution function of the low-density state has both orientational and molecular-density dependencies. The magnitude of  $\gamma$  determines the degree of the curvature-driven nematic distribution. We call this an isotropic-like state, to be distinguished from a

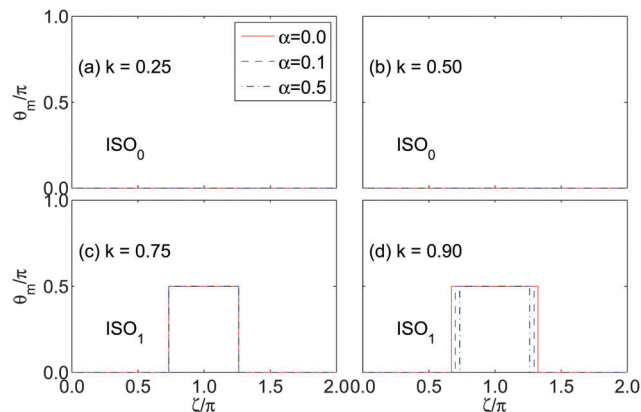


Fig. 2 The nematic-director angle  $\theta_m$  as a function of  $\zeta$  of an isotropic-like state at a low- $\sigma$  case ( $\sigma = 3.0$ ,  $\gamma = 1.0$ ) for various  $\alpha$ .

strong nematic state, driven from the directionally dependent Onsager interaction.

Even in this simple example, the main nematic director of the weak nematic ordering displays an interesting variation as a function of  $k$ . In the small- $k$  regime, the square curvature in (17) has a minimum at  $\theta = 0$ . According to (35), the nematic director on the entire surface is along this direction. In the  $k \geq 1/2$  regime, the square curvature in (17) has a minimum at  $\theta = 0$  when  $\zeta = \pi/2$  and a minimum at  $\theta = \pi/2$  when  $\zeta = \pi$ . Hence the nematic director changes from  $\theta_m = 0$  to  $\theta_m = \pi/2$  somewhere between  $\zeta = \pi/2$  and  $\zeta = \pi$  in a  $k \geq 1/2$  system, all within the same state. In a short summary, we have:

(a) ISO<sub>0</sub> state. In a  $k < 1/2$  system,  $\theta_m = 0$  on the entire pattern.

(b) ISO<sub>1</sub> state. In a  $k > 1/2$  system,  $\theta_m$  is non-uniform, making a jump at a certain  $\zeta$ , from 0 at  $\zeta = 0$  to  $\pi/2$  at  $\zeta = \pi$ .

This is a typical behavior of low- $\sigma$  systems. Here we show a few more examples by numerically solving SCFT presented in Section 2.2. The curves in Fig. 2 represent this behavior for systems at  $\sigma = 3$ ,  $\gamma = 1$ , and various  $\alpha$ . To demonstrate the general ideas, in the first and second columns of Fig. 3, we illustrate a typical directionally ordered pattern, using short straight lines to represent the nematic director  $\mathbf{n}$  and color to represent the density and order-parameter variations. In general, the division of the two  $k$  regimes, ISO<sub>0</sub> and ISO<sub>1</sub>, is always found at  $k \geq 1/2$  for a system of any  $\alpha$  value. The stability of these states can be determined from numerically solving SCFT and then comparing the free energies associated with each branch of solutions.

### 3.4 Defect-free nematic states

At a high density  $\sigma$ , a defect-free nematic state can be found from solving SCFT, where the orientational order parameter is significantly large on the entire toroidal surface. The conformation of the system has a rotational symmetry about the  $z$  axis shown in Fig. 1. As such, all structural properties are functions of  $\zeta$  and  $\theta$  only and are independent of  $\xi$ . Examples of typical order parameter fields are illustrated in Fig. 3(c), (d), and (e).

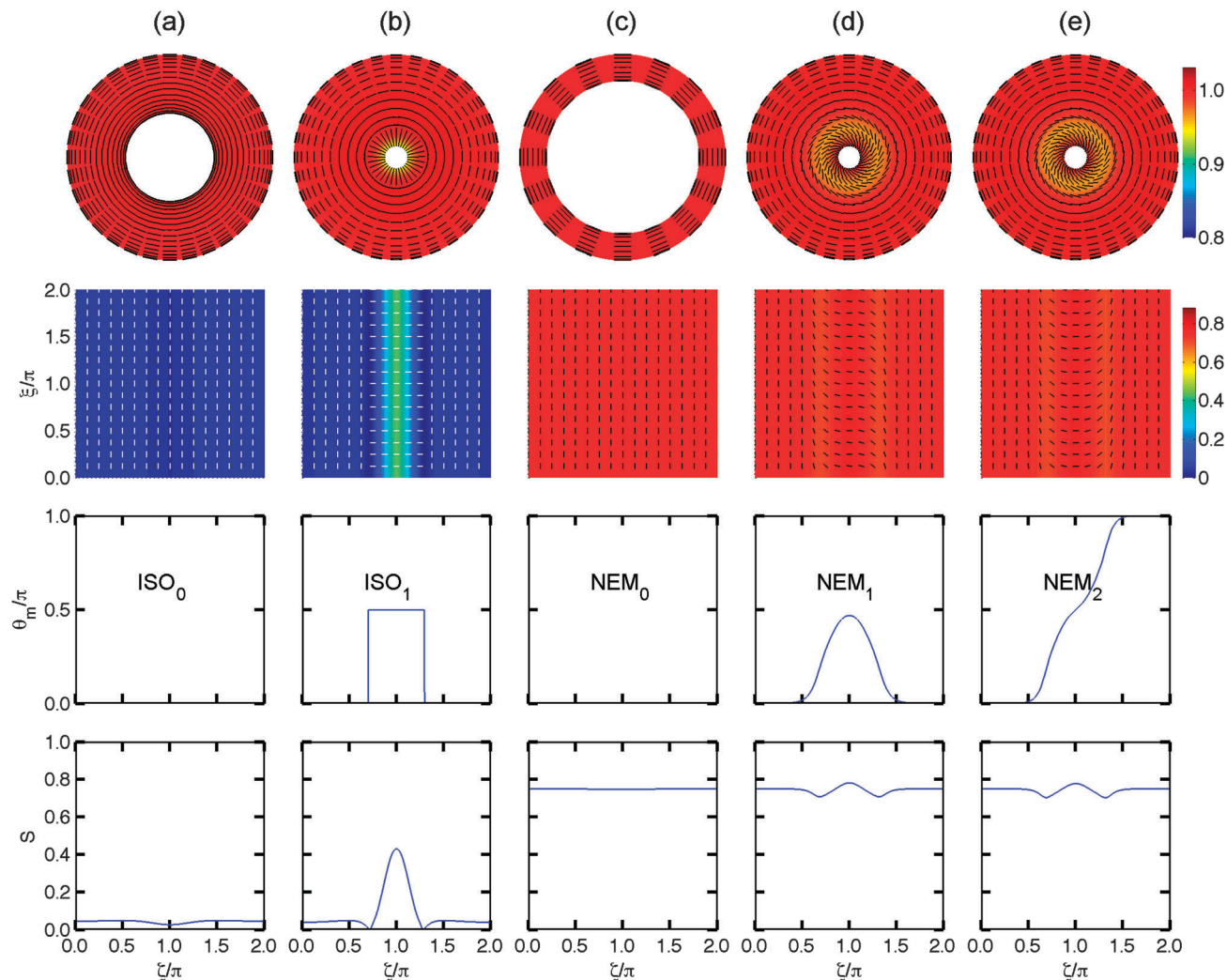


**Fig. 3** The five defect-free states that have no  $\zeta$ -dependence: (a) isotropic-like, ISO<sub>0</sub> (at  $\alpha = 0.1$ ,  $\gamma = 0.1$ ,  $k = 0.4$  and  $\sigma = 2.5$ ), (b) isotropic-like, ISO<sub>1</sub> (at  $\alpha = 0.1$ ,  $\gamma = 0.1$ ,  $k = 0.8$ , and  $\sigma = 2.5$ ), (c) nematic, NEM<sub>0</sub> (at  $\alpha = 0.1$ ,  $\gamma = 0.1$ ,  $k = 0.15$  and  $\sigma = 6.0$ ), and (d) nematic, NEM<sub>1</sub> (at  $\alpha = 0.1$ ,  $\gamma = 0.1$ ,  $k = 0.8$ , and  $\sigma = 6.0$ ), and (e) nematic NEM<sub>2</sub> (at  $\alpha = 0.1$ ,  $\gamma = 0.1$ ,  $k = 0.8$ , and  $\sigma = 6.0$ ). The conformation for every case is shown by four methods: top-torus view (looking down from the  $z$ -axis, see Fig. 1), expanded view by using  $\xi$  and  $\zeta$  as coordinates, nematic-director angle  $\theta_m$  as a function of  $\zeta$ , and order parameter  $S$  as a function of  $\zeta$ . The color on the top-torus view represents the magnitude of the density distribution  $\phi(\xi, \zeta)$ , and the color on the expanded view the order parameter  $S(\xi, \zeta)$ . Short straight bars are added to the color plots to illustrate the nematic directors and they should not be confused with the actual presence of molecules. The selected parameters,  $\alpha = 0.1$  and  $\gamma = 0.1$ , correspond to  $L/r = 0.2$  – the rod-like molecules have a length that is much shorter compared to the toroidal tube radius  $r$ .

As it turns out, there exist at least three defect-free nematic states as listed below:

(a) NEM<sub>0</sub> state. In a low- $k$  parameter regime,  $\theta_m = 0$  over the entire toroidal surface. What differs from the ISO<sub>0</sub> state is the strong nematic order parameter  $S$ . All three cases of Fig. 4(a) and one case of Fig. 4(b) ( $\alpha = 0.5$ ) are examples of this state. A typical configuration is demonstrated in Fig. 3(c).

(b) NEM<sub>1</sub> state. This state emerges in a moderate  $k$  system where a nonzero  $\theta_m$  appears at  $\zeta = \pi$ . Unlike ISO<sub>1</sub>, the variation of  $\theta_m$  as a function of  $\zeta$  becomes smooth, as shown by the examples in Fig. 4. A typical configuration is demonstrated in Fig. 3(d). The director field in this plot has the symmetry  $\theta_m(\xi, \zeta) = \theta_m(\xi, 2\pi - \zeta)$ . Ref. 21, 31 and 32 have all identified the existence of this state.

(c) NEM<sub>2</sub> state. This is a state typically seen in a high- $k$  system where  $\theta_m$  is always  $\pi/2$  at  $\zeta = \pi$ . The director field in this plot has the symmetry  $\theta_m(\xi, \zeta) = \pi - \theta_m(\xi, 2\pi - \zeta)$ . The variation shown in Fig. 5 is different from the symmetry of the NEM<sub>1</sub> state. It has the same symmetry as the first excited state  $\theta_2$  described in ref. 21. As we discuss below, here we found that it can be energetically degenerate to coexist with NEM<sub>1</sub> in some parameter regime. A typical configuration is demonstrated in Fig. 3(e).

Other  $\zeta$ -independent, defect-free nematic configurations can also be stabilized. The characteristic of NEM<sub>1</sub> and NEM<sub>2</sub> is such that as  $\zeta$  varies from 0 to  $2\pi$ ,  $\theta_m$  varies by an angle 0 and  $\pi$ , respectively. Our numerical solution shows that a defect-free nematic state NEM<sub>n</sub> exists such that as  $\zeta$  varies from 0 to  $2\pi$ ,  $\theta_m$

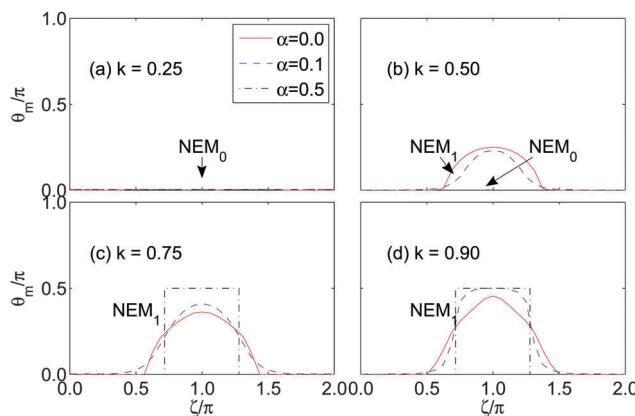


Fig. 4 The nematic-director angle  $\theta_m$  as a function of  $\zeta$  of the NEM<sub>0</sub> and NEM<sub>1</sub> states at a high- $\sigma$  case ( $\sigma = 4.5$ ,  $\gamma = 1.0$ ).

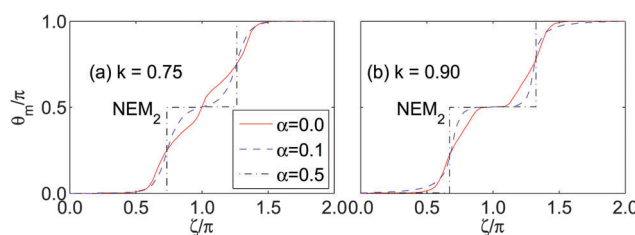


Fig. 5 The nematic-director angle  $\theta_m$  as a function of  $\zeta$  of the NEM<sub>2</sub> state at a high- $\sigma$  case ( $\sigma = 4.5$ ,  $\gamma = 1.0$ ).

varies by an angle  $(n - 1)\pi$ . The states with higher  $n$  ( $\geq 3$ ) are metastable.

### 3.5 Phase transition

To understand the stable phases of the current system, we plot the phase diagram as a function of  $k$  and  $\sigma$ , after specifying values of two other parameters  $\alpha$  and  $\gamma$ . All stable states discussed in preceding sections are summarized in the phase diagram.

To start, we present three phase diagrams on the left column for  $\gamma = 0$  and different values of  $\alpha$ . Here is a special case where all curvature-related features are erased. The system undergoes a transition from the ideal, uniform isotropic phase where  $S = 0$  to an ideal, uniform nematic phase where  $S \neq 0$ . The transition density  $\sigma^*$  of the second-order transition line is given in point (b) of Section 3.1. The nematic director can take any directions on the toroidal surface. This scenario is consistent with the nematic texture described by Evans, after the removal of the bending energy penalty term in (22).<sup>21,28</sup>

Characteristically different from the  $\gamma = 0$  case are the systems with a finite  $\gamma$ . The transition between the isotropic-like states and the nematic states is now first order at sufficiently strong  $\sigma$ . The different branches of the free energy cross each other at the transition point. The finiteness of  $\gamma$  generally encourages nematic ordering, even at low  $\sigma$ . As the consequence, the isotropic state has a weak nematic feature as discussed above and the isotropic-nematic transition phase boundaries move to a lower  $\sigma$  regime. Following the trend of how these phase boundaries

move in Fig. 6, we can conjecture that the isotropic-like region on the phase diagram diminishes in a large  $\gamma$  system.

For convenience we highlight the phase regions in the phase diagram according to properties of a particular state as we addressed in the previous sections.

(a) Low- $k$  systems (grey areas on the phase diagram). The nematic directors are all uniform, pointing to the direction represented by  $\theta_m = 0$ .

(b)  $k \rightarrow 1$  systems (line-shaded areas on the phase diagram). The toroidal surface close to the  $z$  axis has a much greater, directionally dependent curvature; this dependence yields a non-uniform  $\theta_m$  on the surface and in particular a nematic director angle  $\theta_m = \pi/2$  at  $\zeta = \pi$ . The variation of the nematic director on the toroidal surface, however, now has two possibilities: NEM<sub>1</sub> and NEM<sub>2</sub> states are degenerate in this phase region. In the former case, beyond  $\zeta = \pi$ , the angle  $\theta_m$  varies back to 0 from  $\pi/2$ . In the latter case, beyond  $\zeta = \pi$ , the angle  $\theta_m$  reaches a higher value from  $\pi/2$  [see Fig. 3(d) and (e)].

(c) Mid- $k$  systems (unshaded area). A large phase region in the middle is occupied by the NEM<sub>1</sub> state. The nematic director makes an angle  $\theta_m \neq \pi/2$  at  $\zeta = \pi$ . Although the NEM<sub>2</sub> state could be stabilized in this region, it has a higher free energy hence is metastable only.

The coexistence of NEM<sub>1</sub> and NEM<sub>2</sub> in the line-shaded region can be further demonstrated by a plot of the energy difference,  $\beta(F_2 - F_1)/n$  where  $F_1$  and  $F_2$  are the free energies of states NEM<sub>1</sub> and NEM<sub>2</sub>. The triangles in Fig. 7 show this difference as a function of  $k$  for a system at  $\sigma = 7.5$ ,  $\alpha = 0.1$ , and  $\gamma = 0.1$ . Below  $k \simeq 0.80$ , NEM<sub>1</sub>, which has an angle  $\theta_m \neq \pi/2$  at  $\zeta = \pi$ , is energetically preferred. At  $k \simeq 0.80$ , the angle  $\theta_m$  smoothly rises from a lower  $\zeta$  to  $\pi/2$  at  $\zeta = \pi$ . The free energies of NEM<sub>1</sub> and NEM<sub>2</sub> become equal. Above  $k \simeq 0.80$ , these two states are energetically degenerate.

The first-order nature of the transition is determined in this work by examining crossing of two branches of the free energy, each associated with one phase. The state that has the lower free energy is deemed stable. One can, on the other hand, understand the first-order nature on the basis of a symmetry analysis. Consider a given position on a flat two-dimensional surface ( $\gamma = 0$ ) where the nematic state is described by a nonzero  $S = \langle \cos[2(\theta - \theta_m)] \rangle$ . Now, if we rotate the entire plane by  $\pi/2$  about the plane normal,  $S \rightarrow -S$ . Because the system is still the same hence the free energy at this point is the same. This gives rise to a Landau expansion in terms of even powers of  $S$ ; the transition is then second order. This transformation, however, is unavailable on toroidal surface. At a given point in most region, the change of  $S \rightarrow -S$  gives rise to different curvature-generated energy penalties. The free energy hence is not an even function of  $S$ . Thus the transition between the isotropic-like and nematic states is of first order.

Finally, we remark that under otherwise the same physical conditions (that is, fixing  $\gamma$ ,  $\sigma$ , and  $k$ ), a nematic state of a system with a larger  $\alpha$  has weaker directional ordering (that is, a smaller overall  $S$ ). This can be inferred directly from a series of plots in Fig. 6, by an examination of phase diagrams vertically. Take (c4), (b4), and (a4) for example. When  $\alpha$  changes from 0.0,

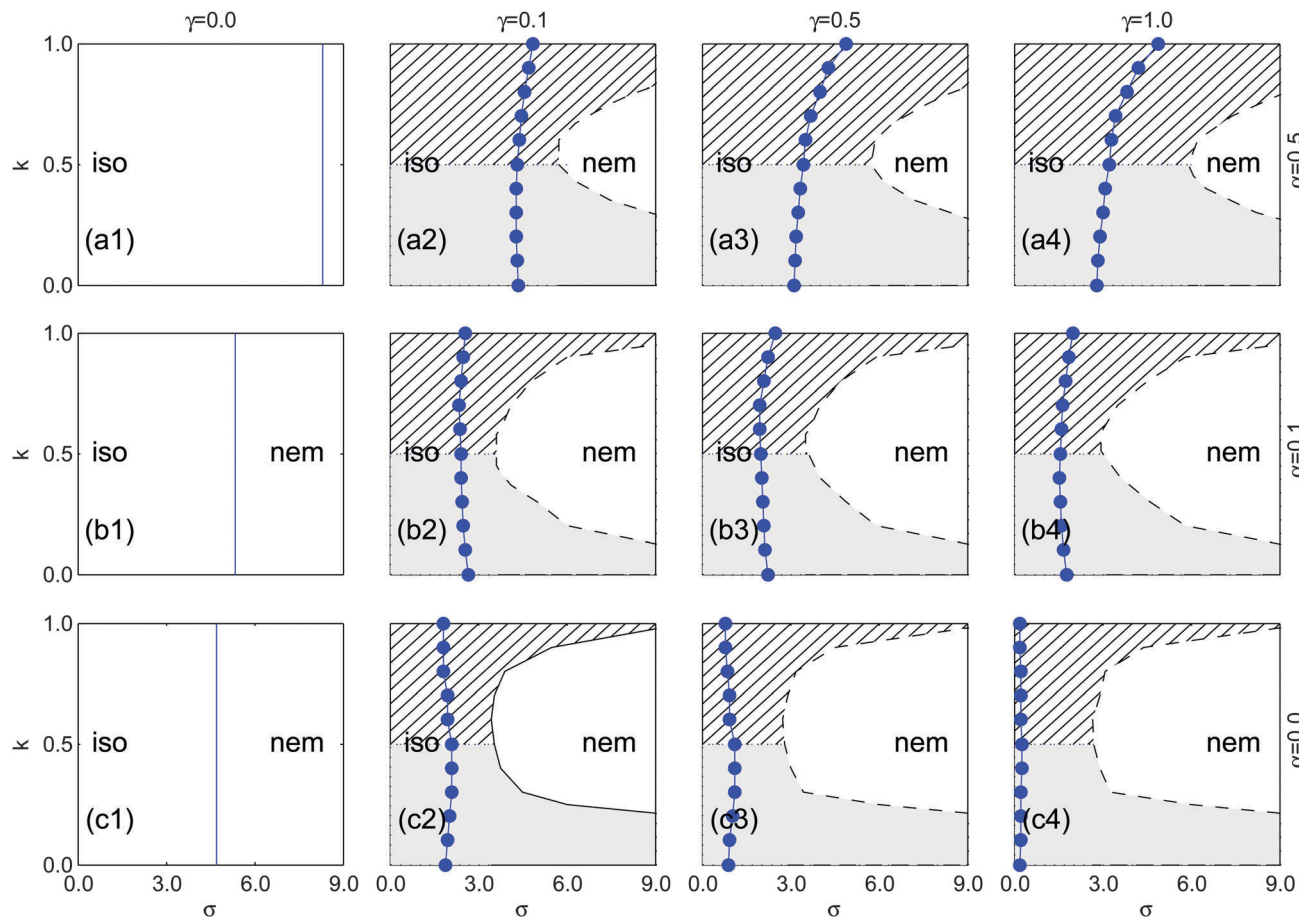


**Fig. 6** Phase diagram yielded from the current model as a function of the four system parameters explained in Section 3.1,  $k$ ,  $\sigma$ ,  $\alpha$ , and  $\gamma$ . The boundary lines on the left column are the second order transition lines. The solid curve behind the circles are first order boundaries. The grey regions are either  $\text{ISO}_0$  or  $\text{NEM}_0$  states and the other regions are either  $\text{ISO}_1$  or  $\text{NEM}_1$  states, depending on the location. In the line-shaded regions  $\text{NEM}_1$  has an energetically degenerate  $\text{NEM}_2$  state. In the unshaded area, the nematic state is  $\text{NEM}_1$  and  $\text{NEM}_2$  is a metastable state. Fig. 3 demonstrates a few examples of these states.

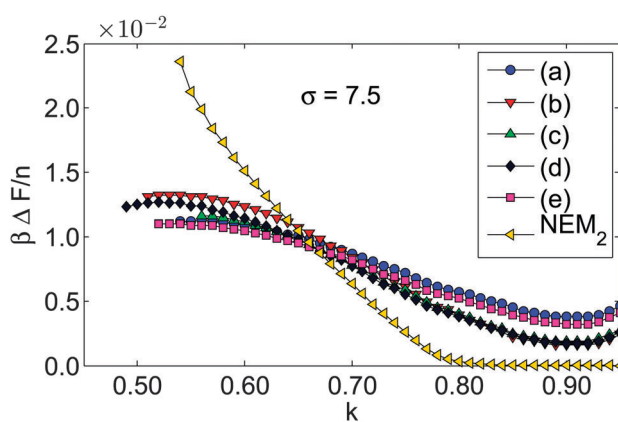


**Fig. 7** Here  $\beta\Delta F = \beta(F - F_1)$ ,  $F_1$  is the corresponding free energy of  $\text{NEM}_1$ . The energy of these defect structures are higher than the energy of  $\text{NEM}_1$ , and they are only stable in a small region of  $k$ .  $\alpha = 0.1$ ,  $\gamma = 0.1$ .

0.1, to 0.5, the isotropic regions expand and nematic regions retract, which is a direct sign of how a larger- $\alpha$  system prefers weaker directional ordering. This observation is consistent with

the trend seen in a completely flat system,  $\gamma = 0$ , from (c1), (b1), to (a1). Fig. 4 and 5 display  $\theta_m$ , the angle that the nematic director makes with respect to  $\xi$ , which indicate another interesting effect of varying  $\alpha$ . In a more rigid system ( $\alpha = 0$ ), the nematic texture is harder to bend hence the variation of  $\theta_m$  is more gradual. In a more flexible system ( $\alpha = 0.5$ ) where the overall nematic ordering is weaker, the nematic texture can more easily bend hence the variation of  $\theta_m$  is step-function alike. Note that the higher maximal value of  $\theta_m$ , seen in Fig. 4(c) and (d) of the  $\alpha = 0.5$  case, is not an indication of the strength of the nematic ordering; it is a result of weaker nematic ordering of a larger- $\alpha$  system.

### 3.6 Defect states

So far we focused on the discussion of defect-free states where the distribution function does not explicitly depend on the variable  $\xi$ . As we shall see as the dependence on  $\xi$  is included in our numerical solution, the nematic textures that contain defects can be stabilized. All have higher free energies than the stable, defect-free nematic states discussed above.

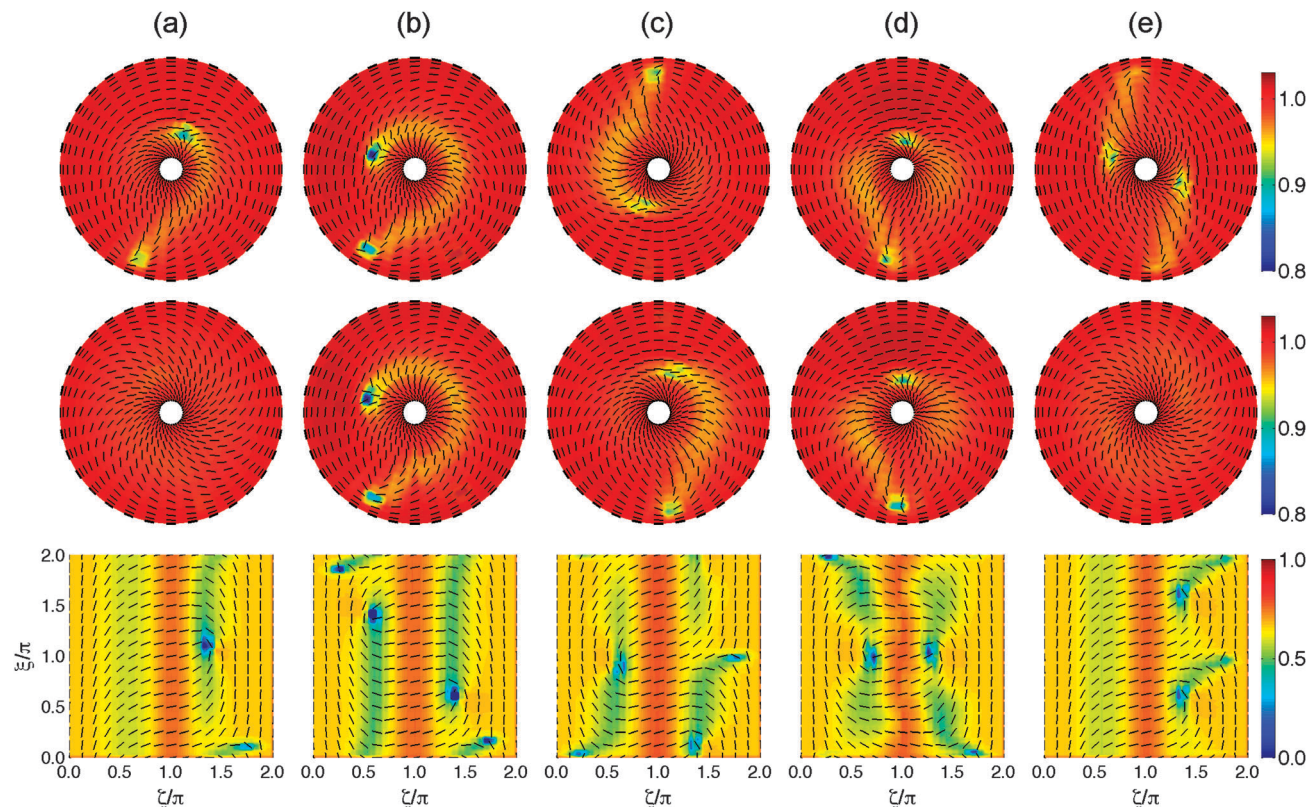


**Fig. 8** Defect patterns that are stabilized from the numerical solutions of the model presented in this work. These patterns are generated from local free energy minimum for a system that has parameter values  $k = 0.8$ ,  $\alpha = 0.1$ ,  $\gamma = 0.1$ ,  $\sigma = 6.0$ . The color on the top-torus view (first row) and back-torus view (second row) represents the number density  $\phi(\xi, \zeta)$  and the color on the expanded view (third row) represents  $S(\xi, \zeta)$ . Defects can be identified by the blue color on the figure ( $S \sim 0$ ).

A few examples of the defect textures are shown in Fig. 8 where top-torus, back-torus, and expanded views are shown. We have produced these structures by numerically solving SCFT with initial guesses that are designed to follow a specific symmetry pattern, or by random initial conditions. Defect points always emerge by pairs, which have  $+1/2$  and  $-1/2$  winding numbers.<sup>2</sup> Fig. 8(a) shows a structure that contains one pair of defects; the defect location and nematic-director-field symmetry completely agree with the structures in Fig. 2(b) of ref. 30, in Fig. 5(a) of ref. 21 (both based on the Frank-energy model). Other patterns in Fig. 8, each displaying a specific symmetry, contain two pairs of defects. The pattern in Fig. 8(c) agrees with the ones shown in Fig. 5(b) of ref. 21 (based on the Frank-energy model) and in Fig. 8(c) of ref. 32 (based on Landau-de Gennes model). The front view of the patterns in Fig. 8(c) or (d) agrees with the pattern shown in Fig. 2(c) of ref. 30 (which does not have the back view). All other defect patterns are newly generated from this work. According to the Poincaré-Hopf theorem, on the torus surface the total winding number as the summation of individual contributions, should be zero.<sup>18</sup> An analysis of the winding numbers of these patterns indicates that the nature of the defects found from the numerical solution completely agrees with the theorem. Overall, Fig. 8 contains defect patterns that were previously determined in the literature, under similar physical conditions. We have not

produced defect patterns that contain more than two pairs of defects<sup>29</sup> but believe that they can also be produced from the current model with a calculation that has a better numerical accuracy.

Nelson and Peliti made an interesting comparison between electrostatics and surface nematic field containing disclinations;<sup>56</sup> the topological defect on a curved surface behaves in a way similar to a charge in an electrostatic problem. Within this analogy, the positive Gaussian curvature plays the role of a negative charge distribution and a topological defect with a positive winding number plays the role of a positive point-like charge. Hence, the high positive Gaussian curvature region attracts a disclination with a positive winding number. A common feature of these defect patterns is that the  $\frac{+1}{2}$  defects are located far away from the  $z$  axis where the Gaussian curvature is positive, whereas the  $\frac{-1}{2}$  defects are closer to the  $z$  axis, where the Gaussian curvature is negative.

To find the defect locations, here we considered the continuous distribution functions such as  $\phi(\xi, \zeta; \theta)$  and  $q(\xi, \zeta; \theta)$ , in a numerical representation of the continuous distribution function. The location of the defects has a low order parameter  $S \sim 0$  which is represented by the blue color in Fig. 8. This can be contrasted with a typical model based on the director vector field, either the nematic director field in ref. 21 or the XY-spin-model realization of the nematic director field in ref. 30;

in these approaches, the defect positions are related to disclinations in the corresponding vector field. In a typical numerical treatment, within the vector representation, the derivatives in the Frank energy model become undefined at the disclination point. A continuous model, such as current SCFT, does not have this difficulty.

As a metastable state, a defect pattern has a higher free energy than that of the stable nematic state. Fig. 7 shows examples of the difference between the free energy per chain of a defect state and that of NEM<sub>1</sub> for  $\alpha = 0.1$ ,  $\gamma = 0.1$  and  $\sigma = 7.5$ . The corresponding defect patterns are shown in Fig. 8. All these defect patterns contain point-like defects that are localized. In the vicinity of a defect, locally the configuration creates a higher free energy, in comparison with the configuration in the same regime of the NEM<sub>1</sub> state. In the low- $k$  regime, the configurations near the entire  $\zeta = \pi$  line of the NEM<sub>2</sub> state create a high local energy cost; hence a defect-free state could have a free energy higher than a defective state.

## 4 Summary

In this paper, we start with a simple density-functional theory, at the same level as the Onsager model for lyotropic rods, to study the stable nematic structures of wormlike chains confined on a toroidal surface. All structures are analyzed by minimization the total free energy of the system.

The model is based on the molecular-level physics, rather than phenomenological concept such as the Frank-energy model<sup>21,28,30,31</sup> and the Landau-de Gennes model for the  $Q$  tensor.<sup>32</sup> The bending energy contribution to the liquid-crystal free energy on a curved surface is a subject that has been highlighted in the literature as a focal point, but mostly based on the one-constant Frank-energy model. The current approach provides a new insight into such an energy contribution – the embedding of molecules on the curved surface gives rise to a term that is proportional to the square normal curvature along the molecular direction. Although this term differs from the surface bending energy contribution deduced from the Frank energy model, some features of the resulting structural properties from the two approaches are similar.

The connection between the current approach and the Frank energy needs to be further clarified and is beyond the scope of the current paper. Various previous attempts have been made to connect molecular-level based model with the Frank energy for a liquid crystal system. For three-dimensional nematics, the Frank constants were deduced from the Flory-Onsager model.<sup>57</sup> One good starting point would be to use a trial function describing the angular distribution about a vector director field  $\mathbf{n}(\mathbf{r})$ . An expansion of the Onsager free energy for rods in terms of the first spatial derivatives, exactly recovered the structure of the Frank energy.<sup>58,59</sup>

The interplay between the four system parameters yields isotropic-like and nematic states in the system. We describe the four-parameter phase space by a series of phase diagrams, which cover a majority phase regime that concerns us. An important

parameter is the reduced number density of molecules on the surface,  $\sigma$ . This is the coefficient of the Onsager interaction term, which drives the system to make orientational ordering at high density, to reduce the excluded-volume interaction. The appearance of such a parameter is typical in a theory for lyotropic system. However, we are not restricted to a lyotropic system here. The coefficient should be regarded more broadly as the coefficient that drives the system to make orientational ordering. The Onsager term can be replaced by the Maier-Saupe interaction energy, for example; in this case, we have a phenomenological coefficient to represent the magnitude of the Maier-Saupe term. The Maier-Saupe coefficient can have temperature or/and density dependencies to describe thermotropic and lyotropic systems. A similar physical picture is expected here.

## References

- 1 T. C. Lubensky and J. Prost, *J. Phys. II*, 1992, **2**, 371–382.
- 2 D. R. Nelson, *Defects and geometry in condensed matter physics*, Cambridge University Press, 2002.
- 3 A. Arsenault, S. Fournier-Bidoz, B. Hatton, H. Miguez, N. Tetreault, E. Vekris, S. Wong, S. Ming Yang, V. Kitaev and G. A. Ozin, *J. Mater. Chem.*, 2004, **14**, 781–794.
- 4 F. Li, W. C. Yoo, M. B. Beernink and A. Stein, *J. Am. Chem. Soc.*, 2009, **131**, 18548–18555.
- 5 M. J. Bowick and L. Giomi, *Adv. Phys.*, 2009, **58**, 449–563.
- 6 A. Fernández-Nieves, V. Vitelli, A. S. Utada, D. R. Link, M. Márquez, D. R. Nelson and D. A. Weitz, *Phys. Rev. Lett.*, 2007, **99**, 157801.
- 7 T. Lopez-Leon, V. Koning, K. B. S. Devaiah, V. Vitelli and A. Fernandez-Nieves, *Nat. Phys.*, 2011, **7**, 391–394.
- 8 D. R. Nelson, *Nano Lett.*, 2002, **2**, 1125–1129.
- 9 M. Huber and H. Stark, *Europhys. Lett.*, 2005, **69**, 135.
- 10 G. Skačej and C. Zannoni, *Phys. Rev. Lett.*, 2008, **100**, 197802.
- 11 H. Shin, M. Bowick and X. Xing, *Phys. Rev. Lett.*, 2008, **101**, 037802.
- 12 M. A. Bates, *J. Chem. Phys.*, 2008, **128**, 104707.
- 13 S. Dhakal, F. J. Solis and M. Olvera de la Cruz, *Phys. Rev. E: Stat., Nonlinear, Soft Matter Phys.*, 2012, **86**, 011709.
- 14 W.-Y. Zhang, Y. Jiang and J. Z. Y. Chen, *Phys. Rev. Lett.*, 2012, **108**, 057801.
- 15 W.-Y. Zhang, Y. Jiang and J. Z. Y. Chen, *Phys. Rev. E: Stat., Nonlinear, Soft Matter Phys.*, 2012, **85**, 061710.
- 16 Y. Li, H. Miao, H. Ma and J. Z. Y. Chen, *Soft Matter*, 2013, **9**, 11461.
- 17 Q. Liang, S. Ye, P. Zhang and J. Z. Y. Chen, *J. Chem. Phys.*, 2014, **141**, 244901.
- 18 M. P. Do Carmo, *Differential geometry of curves and surfaces*, Prentice-Hall, Englewood Cliffs, NJ, 1976.
- 19 P. Sheng, *Phys. Rev. Lett.*, 1976, **37**, 1059–1062.
- 20 P. Sheng, *Phys. Rev. A: At., Mol., Opt. Phys.*, 1982, **26**, 1610–1617.
- 21 Y. Li, H. Miao, H. Ma and J. Z. Y. Chen, *RSC Adv.*, 2014, **4**, 27471–27480.
- 22 A. Chrzanowska, P. I. C. Teixeira, H. Ehrentraut and D. J. Cleaver, *J. Phys.: Condens. Matter*, 2001, **13**, 4715.

- 23 A. Chrzanowska, *J. Comput. Phys.*, 2003, **191**, 265–281.
- 24 D. de las Heras, E. Velasco and L. Mederos, *J. Chem. Phys.*, 2004, **120**, 4949–4957.
- 25 D. de las Heras, E. Velasco and L. Mederos, *Phys. Rev. E: Stat., Nonlinear, Soft Matter Phys.*, 2009, **79**, 061703.
- 26 A. V. Emelyanenko, S. Aya, Y. Sasaki, F. Araoka, K. Ema, K. Ishikawa and H. Takezoe, *Phys. Rev. E: Stat., Nonlinear, Soft Matter Phys.*, 2011, **84**, 041701.
- 27 J. Z. Y. Chen, *Soft Matter*, 2013, **9**, 10921.
- 28 R. M. Evans, *J. Phys. II*, 1995, **5**, 507–530.
- 29 M. Bowick, D. R. Nelson and A. Traveset, *Phys. Rev. E: Stat., Nonlinear, Soft Matter Phys.*, 2004, **69**, 41102.
- 30 R. L. B. Selinger, A. Konya, A. Traveset and J. V. Selinger, *J. Phys. Chem. B*, 2011, **115**, 13989–13993.
- 31 A. Segatti, M. Snarski and M. Veneroni, *Phys. Rev. E: Stat., Nonlinear, Soft Matter Phys.*, 2014, **90**, 012501.
- 32 D. Jesenek, S. Kralj, R. Rosso and E. G. Virga, *Soft Matter*, 2015, **11**, 2434–2444.
- 33 G. Napoli and L. Vergori, *Phys. Rev. Lett.*, 2012, **108**, 207803.
- 34 G. Napoli and L. Vergori, *Phys. Rev. E: Stat., Nonlinear, Soft Matter Phys.*, 2012, **85**, 061701.
- 35 L. Onsager, *Ann. N. Y. Acad. Sci.*, 1949, **51**, 627–659.
- 36 A. Khokhlov and A. Semenov, *Phys. A*, 1982, **112**, 605–614.
- 37 T. Odijk, *Macromolecules*, 1986, **19**, 2313–2329.
- 38 G. J. Vroege and T. Odijk, *Macromolecules*, 1988, **21**, 2848–2858.
- 39 Z. Y. Chen, *Macromolecules*, 1993, **26**, 3419–3423.
- 40 Z. Y. Chen, *Phys. Rev. E: Stat., Nonlinear, Soft Matter Phys.*, 1993, **47**, 3765–3767.
- 41 Y. Jiang and J. Z. Y. Chen, *Macromolecules*, 2010, **43**, 10668–10678.
- 42 S. Ye, P. Zhang and J. Z. Y. Chen, *Soft Matter*, 2016, **12**, 2948–2959.
- 43 J. Z. Y. Chen, *Prog. Polym. Sci.*, 2016, **54–55**, 3–46.
- 44 N. Saito, K. Takahashi and Y. Yunoki, *J. Phys. Soc. Jpn.*, 1967, **22**, 219.
- 45 A. R. Khokhlov and A. N. Semenov, *Phys. A*, 1982, **112**, 605.
- 46 T. Odijk, *Macromolecules*, 1986, **19**, 2313–2329.
- 47 K. F. Freed, *Adv. Chem. Phys.*, 1972, **22**, 1.
- 48 Q. Liang, J. Li, P. Zhang and J. Z. Y. Chen, *J. Chem. Phys.*, 2013, **138**, 244910.
- 49 F. C. Frank, *Discuss. Faraday Soc.*, 1958, **25**, 19–28.
- 50 P. G. de Gennes and J. Prost, *The Physics of Liquid Crystals*, Clarendon Press, Oxford, 2nd edn, 1993, p. 616.
- 51 Z. Y. Chen, *Phys. Rev. Lett.*, 1993, **71**, 93–96.
- 52 W. Maier and A. Saupe, *Zeitschrift Fur Naturforsch. Part a-Astrophysik Phys. Und Phys. Chemie*, 1959, **14**, 882–889.
- 53 V. V. Rusakov and M. I. Shilomis, *J. Phys., Lett.*, 1985, **46**, L935–L943.
- 54 Y. Jiang, X. Zhang, B. Miao and D. Yan, *J. Chem. Phys.*, 2015, **142**, 154901.
- 55 A. Leferink op Reinink, E. van den Pol, A. Petukhov, G. Vroege and H. Lekkerkerker, *Eur. Phys. J.: Spec. Top.*, 2013, **222**, 3053–3069.
- 56 D. R. Nelson and L. Peliti, *J. Phys.*, 1987, **48**, 1085–1092.
- 57 M. Kleman and O. D. Laverntovich, *Soft Matter Physics: an Introduction*, Springer, 2003.
- 58 J. P. Straley, *Phys. Rev. A: At., Mol., Opt. Phys.*, 1973, **8**, 2181.
- 59 A. Poniewierski and R. Hołyst, *Phys. Rev. A: At., Mol., Opt. Phys.*, 1990, **41**, 6871.